Manuscript submitted to
AIMS' Journals
Volume **X**, Number **0X**, XX **200X**

Website: http://AIMsciences.org

pp. **X–XX**

EFFICIENT AND ACCURATE COMPUTATION OF SPHERICAL MEAN VALUES AT SCATTERED CENTER POINTS

TORSTEN GÖRNER

University Osnabrück, Institute of Mathematics
49069 Osnabrück, Germany

RALF HIELSCHER

University Chemnitz, Department of Mathematics
09107 Chemnitz, Germany

STEFAN KUNIS

University Osnabrück, Institute of Mathematics, 49069 Osnabrück, and
Helmholtz Zentrum München, Institute for Biomathematics and Biometry, 85764 Neuherberg, Germany

(Communicated by the associate editor name)

ABSTRACT. Spherical means are a widespread model in modern imaging modalities like photoacoustic tomography. Besides direct inversion methods for specific geometries, iterative methods are often used as reconstruction scheme such that each iteration asks for the efficient and accurate computation of spherical means. We consider a spectral discretization via trigonometric polynomials such that the computation can be done via nonequispaced fast Fourier transforms. Moreover, a recently developed sparse fast Fourier transform is used in the three-dimensional case and gives optimal arithmetic complexity. All theoretical results are illustrated by numerical experiments.

1. **Introduction.** In analogy to the classical Radon transform, we consider the spherical mean value operator $\mathcal{M}$ that assigns to each function $f\colon \mathbb{R}^d \to \mathbb{R}$ its mean values

$$\mathcal{M}f(\mathbf{y}, r) = \frac{1}{\omega_{d-1}} \int_{\mathbb{S}^{d-1}} f(\mathbf{y} + r\boldsymbol{\xi}) \, \mathrm{d}\sigma(\boldsymbol{\xi})$$

along the spheres with center point $\mathbf{y} \in \mathbb{R}^d$ and radius $r > 0$, where σ denotes the surface measure on the sphere and $\omega_{d-1} = \sigma(\mathbb{S}^{d-1})$. The spherical mean value operator plays an equal prominent role for recent imaging techniques as the classical Radon transform does already for about 50 years. Most notably, the mathematical models behind upcoming hybrid imaging techniques like thermo- and photo-acoustic tomography [26, 18, 4] are based upon the spherical mean value operator. In most cases, the inverse problem is of interest, i.e. given the spherical means $\mathcal{M}f(\mathbf{y}_{m_1}, r_{m_2})$ for a list of center points $\mathbf{y}_{m_1} \in \mathbb{R}^d$, $m_1 = 1, \dots, M_1$, and radii $r_{m_2} \in (0, \infty)$, $m_2 = 1, \dots, M_2$, we aim to reconstruct f from this data. Existence, uniqueness, and stability of this problem has been studied for the two-dimensional case and for specific three-dimensional geometries over the last decade, see e.g. [8, 3, 1, 18, 25] and references therein. Moreover, specific direct reconstruction

2000 *Mathematics Subject Classification.* 65T40, 65T50, 44A12, 92C55.
Key words and phrases. spherical means, trigonometric approximation, fast Fourier transform, tomography.
TG and SK are partially supported by DFG grant KU 2557/1-2 and by the Helmholtz grant VH-NG-526.

algorithms for various geometries are discussed in [14, 22, 21, 13, 2, 7, 20, 9], variants for integrating detectors are discussed in [12, 5, 24, 30, 15, 29].

In this paper we consider the case of center points located at an arbitrary submanifold of $\mathbb{R}^d$. For this general case, explicit inversion formulae are not known and do not represent a realistic goal, see also [23, 10, 11]. Instead we focus on discretizations and fast algorithms for the forward problem such that the well developed machinery of iterative solvers can be applied, see [6] for a specific reconstruction algorithm. Our idea is to restrict the spherical mean value operator to periodic functions and to discretize these by trigonometric interpolation. In particular, this allows for error bounds that depend on the smoothness of the function at hand. Moreover, we show that in the three-dimensional case the discrete spherical mean value operator can be identified with a four-dimensional sparse Fourier transform with nodes and frequencies restricted to some three-dimensional submanifolds. For this setting, the sparse Fourier transform [28, 19] applies and has the numerical complexity $\mathcal{O}(N^3 \log^6 N)$, where N is the number of discretization points in each dimension. This numerical complexity compares favorable to the numerical complexity of a finite element type discretization which is $\mathcal{O}(N^5)$.

The structure of our paper is as follows. Section 2 defines the spherical mean value operator on the torus and proves in Theorem 2.2 a singular value decomposition in the space of square integrable functions. In Section 3, we define the discrete spherical mean value operator by trigonometric interpolation and prove associated error bounds in Theorem 3.1. The representation of the discrete operator as a four-dimensional Fourier transform can be found in Theorem 3.3 and Algorithm 2 is the corresponding fast scheme. In the last section we verify our theoretical findings numerically by considering a family of test functions with known spherical means and known Fourier coefficients. In particular, we show that our algorithms respect the theoretic error bounds and that they outperform the simplest finite element type discretizations, i.e., piecewise constant and bilinear interpolation, with respect to computing time.

2. The spherical mean value operator for periodic functions.

We start by considering the spherical mean value operator on periodic functions and give its singular value decomposition in the space of square integrable functions. Let $d \in \mathbb{N}$, $\mathbf{x}, \mathbf{y} \in \mathbb{R}^d$, and denote by $\mathbf{x} \cdot \mathbf{y} := x_1 y_1 + \ldots + x_d y_d$ and $|\mathbf{x}| := \sqrt{\mathbf{x} \cdot \mathbf{x}}$ the usual inner product and its induced norm, respectively. We define the d-dimensional torus $\mathbb{T}^d := \mathbb{R}^d / \mathbb{Z}^d = [-\frac{1}{2}, \frac{1}{2})^d$ and the unit sphere $\mathbb{S}^{d-1} := \{\mathbf{x} \in \mathbb{R}^d : \mathbf{x} \cdot \mathbf{x} = 1\}$. By $\mathrm{d}\sigma(\boldsymbol{\xi})$ we denote the spherical surface measure and by

$$\omega_{d-1} := \int_{\mathbb{S}^{d-1}} 1 \,\mathrm{d}\sigma(\boldsymbol{\xi}) = \frac{2\pi^{\frac{d}{2}}}{\Gamma\left(\frac{d}{2}\right)} \tag{1}$$

its total area. We define the spherical mean value operator by

$$\mathcal{M} \colon L^p(\mathbb{T}^d) \to L^p(\mathbb{T}^d \times [0,1],\, \mathrm{d}\mathbf{y} r^{d-1}\,\mathrm{d}r), \quad \mathcal{M}f(\mathbf{y}, r) := \frac{1}{\omega_{d-1}} \int_{\mathbb{S}^{d-1}} f(\mathbf{y} + r\boldsymbol{\xi})\,\mathrm{d}\sigma(\boldsymbol{\xi}).$$

The restriction to $r \leq 1$ is for convenience and could be replaced by any other finite number. It should be noted that compactly supported functions fit in our framework by the following consideration. Let $f \in C(\mathbb{R}^d)$ be a compactly supported function with $\operatorname{supp} f \subset \left\{\mathbf{x} \in \mathbb{R}^d : |\mathbf{x}| \leq R\right\}$, $R \in (0, \frac{1}{2})$, and let $\tilde{f} \in C(\mathbb{T}^d)$,

$$\tilde{f}(\mathbf{x}) := \sum_{\mathbf{z} \in \mathbb{Z}^d} f(\mathbf{x} + \mathbf{z}),$$

be the corresponding periodized function. Then $r \leq 1 - R - |\mathbf{y}|$ is a sufficient condition on the support of f, on the location of the center points $\mathbf{y}$, and on the radii r such that the spherical means $\mathcal{M}f(\mathbf{y}, r)$ of the compactly supported function f and the spherical means $\mathcal{M}\tilde{f}(\mathbf{y}, r)$ of the periodic function $\tilde{f}$ agree.

Lemma 2.1. *The spherical mean value operator satisfies*

$$\begin{aligned} \|\mathcal{M}f\|_{L^\infty(\mathbb{T}^d\times[0,1])} &\leq \|f\|_{L^\infty(\mathbb{T}^d)} \quad \textit{and} \\ \|\mathcal{M}f\|_{L^p(\mathbb{T}^d\times[0,1])} &\leq d^{-1/p}\,\|f\|_{L^p(\mathbb{T}^d)}\,,\ 1 \leq p < \infty. \end{aligned}$$

In particular, every $f \in L^2(\mathbb{T}^d)$ has mean values $\mathcal{M}f \in L^2(\mathbb{T}^d \times [0,1],\, \mathrm{d}\mathbf{y} r^{d-1}\,\mathrm{d}r)$.

Proof. The assertion follows for $p = \infty$ right from the definition. For $1 \leq p < \infty$ and $\frac{1}{q} = 1 - \frac{1}{p}$, the Hölder inequality yields

$$\begin{aligned} &\|\mathcal{M}f\|^p_{L^p(\mathbb{T}^d\times[0,1])} \\ &\quad= \int_0^1 \int_{\mathbb{T}^d} \frac{1}{\omega_{d-1}^p} \left| \int_{\mathbb{S}^{d-1}} f(\mathbf{y} + r\boldsymbol{\xi})\,\mathrm{d}\sigma(\boldsymbol{\xi}) \right|^p \mathrm{d}\mathbf{y} r^{d-1}\,\mathrm{d}r \\ &\quad\leq \int_0^1 \int_{\mathbb{T}^d} \frac{1}{\omega_{d-1}^p} \left(\int_{\mathbb{S}^{d-1}} \mathrm{d}\sigma(\boldsymbol{\xi}) \right)^{\frac{p}{q}} \int_{\mathbb{S}^{d-1}} |f(\mathbf{y} + r\boldsymbol{\xi})|^p\,\mathrm{d}\sigma(\boldsymbol{\xi})\,\mathrm{d}\mathbf{y} r^{d-1}\,\mathrm{d}r \\ &\quad= \int_0^1 (\omega_{d-1})^{\frac{p}{q}-p} \int_{\mathbb{S}^{d-1}} \int_{\mathbb{T}^d} |f(\mathbf{y} + r\boldsymbol{\xi})|^p\,\mathrm{d}\mathbf{y}\,\mathrm{d}\sigma(\boldsymbol{\xi}) r^{d-1}\,\mathrm{d}r \\ &\quad= \|f\|^p_{L^p(\mathbb{T}^d)} \int_0^1 r^{d-1}\,\mathrm{d}r = \frac{1}{d}\,\|f\|^p_{L^p(\mathbb{T}^d)}\,. \end{aligned}$$

□

For order $\nu \geq 0$ we define the Bessel functions $\mathcal{J}_\nu \colon \mathbb{R} \to \mathbb{R}$ by the integral representation, cf. [27, Chap. 3.3],

$$\mathcal{J}_\nu(x) := \frac{x^\nu}{\Gamma\left(\nu + \frac{1}{2}\right)\Gamma\left(\frac{1}{2}\right)2^\nu} \int_0^\pi \mathrm{e}^{\mathrm{i}x\cos\xi} (\sin\xi)^{2\nu} \mathrm{d}\xi. \tag{2}$$

We have the following singular value decomposition of the spherical mean value operator in the Hilbert space of square integrable functions. The main part of this result can be found e.g. in [16, Eq. (1.5)] but we present the complete statement together with its short proof to keep the paper self contained.

Theorem 2.2. *For $\mathbf{z} \in \mathbb{Z}^d$, $\mathbf{x}, \mathbf{y} \in \mathbb{T}^d$, and $r \in [0,1]$ we define $v_\mathbf{z}(\mathbf{x}) := \mathrm{e}^{2\pi\mathrm{i}\,\mathbf{z}\cdot\mathbf{x}}$,*

$$\tilde{u}_\mathbf{z}(\mathbf{y}, r) := \mathrm{e}^{2\pi\mathrm{i}\,\mathbf{z}\cdot\mathbf{y}} \frac{\Gamma\left(\frac{d}{2}\right) \mathcal{J}_{\frac{d-2}{2}}(2\pi\,|\mathbf{z}|\,r)}{(\pi\,|\mathbf{z}|\,r)^{\frac{d-2}{2}}}, \quad \lambda_\mathbf{z} := \|\tilde{u}_\mathbf{z}\|_{L^2(\mathbb{T}^d\times[0,1])}\,, \quad u_\mathbf{z} := \lambda_\mathbf{z}^{-1}\tilde{u}_\mathbf{z}.$$

Then the spherical mean value operator has the singular value decomposition

$$\mathcal{M}v_\mathbf{z} = \lambda_\mathbf{z} u_\mathbf{z}, \quad \mathbf{z} \in \mathbb{Z}^d.$$

Moreover, there are constants $C_1, C_2 > 0$ such that for all $\mathbf{z} \in \mathbb{Z}^d$, $\mathbf{z} \neq \mathbf{0}$, the estimate

$$C_1\,|\mathbf{z}|^{\frac{1-d}{2}} \leq \lambda_\mathbf{z} \leq C_2\,|\mathbf{z}|^{\frac{1-d}{2}} \tag{3}$$

is valid.

Proof. The functions $v_{\mathbf{z}}$, $\mathbf{z} \in \mathbb{Z}^d$, form a complete orthonormal system in $L^2(\mathbb{T}^d)$ and the functions $u_{\mathbf{z}}$, $\mathbf{z} \in \mathbb{Z}^d$, form an orthonormal system in $L^2(\mathbb{T}^d \times [0,1], \mathrm{d}\mathbf{y} r^{d-1}\,\mathrm{d}r)$. For $\mathbf{z} \in \mathbb{Z}^d$ we have to compute

$$\mathcal{M}v_{\mathbf{z}}(\mathbf{y}, r) = \frac{1}{\omega_{d-1}} \int_{\mathbb{S}^{d-1}} \mathrm{e}^{2\pi \mathrm{i} \mathbf{z}\cdot(\mathbf{y}+r\boldsymbol{\xi})}\,\mathrm{d}\sigma(\boldsymbol{\xi}) = \mathrm{e}^{2\pi \mathrm{i}\, \mathbf{z}\cdot\mathbf{y}} \frac{1}{\omega_{d-1}} \int_{\mathbb{S}^{d-1}} \mathrm{e}^{2\pi\,\mathrm{i}\, r\, \boldsymbol{\xi}\cdot\mathbf{z}}\,\mathrm{d}\sigma(\boldsymbol{\xi}).$$

Let $\boldsymbol{\zeta} := \frac{\mathbf{z}}{|\mathbf{z}|}$ and denote by $\boldsymbol{\zeta}^\perp := \{\boldsymbol{\eta} \in \mathbb{S}^{d-1} : \boldsymbol{\eta} \perp \boldsymbol{\zeta}\}$ the set of unit vectors orthogonal to $\boldsymbol{\zeta}$. Then, using polar coordinates $\boldsymbol{\xi} = \sin\theta\,\boldsymbol{\eta} + \cos\theta\,\boldsymbol{\zeta}$, $\theta \in [0,\pi]$, $\boldsymbol{\eta} \in \boldsymbol{\zeta}^\perp$, with respect to the north pole $\boldsymbol{\zeta} \in \mathbb{S}^{d-1}$, we can write the $(d-1)$-dimensional surface measure $\mathrm{d}\sigma(\boldsymbol{\xi}) = (\sin\theta)^{d-2}\,\mathrm{d}\tilde{\sigma}(\boldsymbol{\eta})\,\mathrm{d}\theta$ in terms of the $(d-2)$-dimensional surface measure $\mathrm{d}\tilde{\sigma}$ on $\boldsymbol{\zeta}^\perp$. With the definition of the Bessel function (2), this yields

$$\begin{aligned}
&\frac{1}{\omega_{d-1}} \int_{\mathbb{S}^{d-1}} \mathrm{e}^{2\pi\,\mathrm{i}\, r|\mathbf{z}|\,\boldsymbol{\xi}\cdot\boldsymbol{\zeta}}\,\mathrm{d}\sigma(\boldsymbol{\xi}) \\
&\quad= \frac{1}{\omega_{d-1}} \int_0^\pi \int_{\boldsymbol{\eta}\in\boldsymbol{\zeta}^\perp} \mathrm{e}^{2\pi\,\mathrm{i}\, r|\mathbf{z}|\,\boldsymbol{\zeta}\cdot(\cos\theta\,\boldsymbol{\zeta}+\sin\theta\,\boldsymbol{\eta})} (\sin\theta)^{d-2}\,\mathrm{d}\tilde{\sigma}(\boldsymbol{\eta})\,\mathrm{d}\theta \\
&\quad= \frac{\omega_{d-2}}{\omega_{d-1}} \int_0^\pi \mathrm{e}^{2\pi\,\mathrm{i}\, r|\mathbf{z}|\,\cos\theta} (\sin\theta)^{d-2}\,\mathrm{d}\theta \\
&\quad= \frac{\Gamma\left(\frac{d}{2}\right)}{\sqrt{\pi}\Gamma\left(\frac{d-1}{2}\right)} \cdot \frac{\Gamma\left(\frac{d-1}{2}\right)\Gamma\left(\frac{1}{2}\right) \mathcal{J}_{\frac{d-2}{2}}(2\pi|\mathbf{z}|r)}{(\pi|\mathbf{z}|r)^{\frac{d-2}{2}}} \\
&\quad= \Gamma(\tfrac{d}{2}) \cdot \frac{\mathcal{J}_{\frac{d-2}{2}}(2\pi\,|\mathbf{z}|\,r)}{(\pi\,|\mathbf{z}|\,r)^{\frac{d-2}{2}}}.
\end{aligned}$$

Since the functions $\tilde{u}_{\mathbf{z}}$, $\mathbf{z} \in \mathbb{Z}^d$, are orthogonal in $L^2(\mathbb{T}^d \times [0,1], d\mathbf{y} r^{d-1}\,\mathrm{d}r)$ the singular value decomposition is shown.

Next we consider the singular values $\lambda_{\mathbf{z}}$, $\mathbf{z} \in \mathbb{Z}^d$, which fulfill

$$\lambda_{\mathbf{z}}^2 = \|\tilde{u}_{\mathbf{z}}\|^2_{L^2(\mathbb{T}^d\times[0,1])} = \frac{\left(\Gamma(\frac{d}{2})\right)^2}{\pi^{d-2}\,|\mathbf{z}|^d} \int_0^{|\mathbf{z}|} \mathcal{J}_{\frac{d-2}{2}}(2\pi r)^2 r\,\mathrm{d}r. \tag{4}$$

From the asymptotic expansion of the Bessel functions [27, Sec. 7.21] we know that there is a constant $C_3 > 0$ such that for all $r > 0$ we have

$$\left| \mathcal{J}_{\frac{d-2}{2}}(r) - \left(\frac{2}{\pi r}\right)^{1/2} \cos\left(r - \frac{d-3}{4}\pi\right) \right| \le C_3 r^{-3/2}. \tag{5}$$

Thus, the integral in Equation (4) can be bounded by

$$\begin{aligned}
\int_0^{|\mathbf{z}|} \mathcal{J}_{\frac{d-2}{2}}(2\pi r)^2 r\,\mathrm{d}r &\le C_4(\varepsilon) + \int_\varepsilon^{|\mathbf{z}|} \mathcal{J}_{\frac{d-2}{2}}(2\pi r)^2 r\,\mathrm{d}r \\
&\le C_4(\varepsilon) + \int_\varepsilon^{|\mathbf{z}|} \frac{2}{\pi r} \cos(2\pi r - \tfrac{d-3}{4}\pi)^2 r\,\mathrm{d}r + C_5 \int_\varepsilon^{|\mathbf{z}|} r^{-3} r\,\mathrm{d}r \\
&\le C_4(\varepsilon) + C_6\,|\mathbf{z}| + C_5/\varepsilon
\end{aligned}$$

which gives the upper bound. The lower bound follows analogously. □

3. **Discretization.** Typically, the function $f : \mathbb{T}^d \to \mathbb{R}$ is given by discrete values $f(\mathbf{x_n})$ on a regular grid $\mathbf{x_n} \in X \subset \mathbb{T}^d$ and the spherical means $\mathcal{M}f(\mathbf{y}, r)$ have to be computed for scattered center points $\mathbf{y} \in \mathbb{T}^d$ and radii $r \in (0,1]$. Subsequently, we suggest to compute an expansion into complex exponentials from the given data, then apply Theorem 2.2 which gives precise information about the spherical means of a complex exponential

function, and finally perform a summation step to compute the spherical means of the complete expansion at the scattered center points.

We start by defining for some discretization parameter $N \in 2\mathbb{N}$ the index sets

$$I_N := [0, N)^d \cap \mathbb{Z}^d, \quad J_N := \left[-\frac{N}{2}, \frac{N}{2}\right)^d \cap \mathbb{Z}^d,$$

and within the torus $\mathbb{T}^d = [-\frac{1}{2}, \frac{1}{2})^d$ the sampling grid

$$X := \left\{\mathbf{x_n} \in \mathbb{T}^d : \mathbf{x_n} = \left(\tfrac{2n_1+1-N}{2N}, \ldots, \tfrac{2n_d+1-N}{2N}\right), \mathbf{n} \in I_N\right\}.$$

Moreover, let T_N be the space of trigonometric polynomials $p : \mathbb{T}^d \to \mathbb{C}$,

$$p(\mathbf{x}) = \sum_{\mathbf{z} \in J_N} \hat{p}_{\mathbf{z}} \mathrm{e}^{2\pi \mathrm{i} \mathbf{z}\cdot\mathbf{x}}, \quad \hat{p}_{\mathbf{z}} \in \mathbb{C},$$

and define the corresponding interpolation operator $\mathcal{I}_N : C(\mathbb{T}^d) \to T_N$, $f \mapsto \mathcal{I}_N f = p$,

$$p(\mathbf{x}) = f(\mathbf{x}), \quad \mathbf{x} \in X.$$

For subsequent use, we define the vector of samples $\mathbf{f} \in \mathbb{R}^{N^d}$, $\mathbf{f} := f(\mathbf{x})$, $\mathbf{x} \in X$. The Fourier coefficients of the interpolating trigonometric polynomial are given by

$$\hat{p}_{\mathbf{z}} = \frac{1}{N^d} \sum_{\mathbf{x} \in X} f(\mathbf{x}) \mathrm{e}^{-2\pi \mathrm{i} \mathbf{x}\cdot\mathbf{z}}, \quad \mathbf{z} \in J_N, \tag{6}$$

and can be computed from the samples by means of the fast Fourier transform (FFT). Moreover, sufficiently smooth functions $f(\mathbf{x}) = \sum_{\mathbf{k} \in \mathbb{Z}} \hat{f}_{\mathbf{z}} \mathrm{e}^{2\pi \mathrm{i} \mathbf{z}\cdot\mathbf{x}}$ allow for a simple bound on the interpolation error, see e.g. [31, Chap. X, Thm. (5.16)],

$$\|f - \mathcal{I}_N f\|_{L^\infty(\mathbb{T}^d)} \leq 2 \sum_{\mathbf{z} \in \mathbb{Z}^d \setminus J_N} \left|\hat{f}_{\mathbf{z}}\right|. \tag{7}$$

Remark 1. The trigonometric polynomial p interpolates on the symmetric spatial grid $X \subset \mathbb{T}^d$ with an even number $N \in 2\mathbb{N}$ of points. For real interpolation values, the computed polynomial is nevertheless complex valued in general but can be modified to a real valued trigonometric polynomial interpolating the data by extending its Fourier coefficients to $[-\frac{N}{2}, \frac{N}{2}]^d \cap \mathbb{Z}^d \supset J_N$ appropriately.

Instead of the trigonometric interpolant we will also use the Fourier partial sum, defined by

$$\mathcal{S}_N f(\mathbf{x}) := \sum_{\mathbf{z} \in J_N} \hat{f}_{\mathbf{z}} \mathrm{e}^{2\pi \mathrm{i} \mathbf{z}\cdot\mathbf{x}}$$

with the true Fourier coefficients $\hat{f}_{\mathbf{z}} = \int_{\mathbb{T}^d} f(\mathbf{x}) \mathrm{e}^{-2\pi \mathrm{i} \mathbf{z}\cdot\mathbf{x}} \mathrm{d}\mathbf{x}$. Given, we only know samples of the function at the nodes X, one is not able to compute these required coefficients. Nevertheless, this variant is useful for theoretical purposes and gives us slightly higher capability to compare the theoretical with the numerical results.

In order to give upper bounds for the resulting errors of our discretization of the spherical mean value operator we introduce for $s > 0$ the Sobolev space $\mathcal{H}_s(\mathbb{T}^d) \subset L^2(\mathbb{T}^d)$ as the subspace of all functions $f \in L^2(\mathbb{T}^d)$ with finite Sobolev norm

$$\|f\|^2_{\mathcal{H}_s(\mathbb{T}^d)} := \sum_{\mathbf{z} \in \mathbb{Z}^d} |\hat{f}_{\mathbf{z}}|^2 \left(1 + (2\pi)^2 |\mathbf{z}|^2\right)^s.$$

For those functions we have the following result.

Theorem 3.1. *Let $d \in \mathbb{N}$, $N \in 2\mathbb{N}$, $N \geq 4\sqrt{d}$, $f \in \mathcal{H}_s(\mathbb{T}^d)$, $\mathbf{y} \in \mathbb{T}^d$, and $r \in (0,1]$ be given. Then for $s > \frac{d}{2}$ the error of the approximated spherical means can be bounded by*

$$|\mathcal{M}f(\mathbf{y},r) - \mathcal{M}\mathcal{I}_N f(\mathbf{y},r)| \leq \frac{2^{s-\frac{d}{2}+1} \cdot \pi^{-s+\frac{d}{4}}}{\sqrt{\Gamma\left(\frac{d}{2}\right) \cdot (2s-d)}} \|f\|_{\mathcal{H}_s(\mathbb{T}^d)} N^{-s+\frac{d}{2}}.$$

Moreover, it exists a constant $C_{f,s,d,r} > 0$ such that for $s > \frac{1}{2}$ the estimate

$$|\mathcal{M}f(\mathbf{y},r) - \mathcal{M}\mathcal{S}_N f(\mathbf{y},r)| \leq \sqrt{\frac{\Gamma\left(\frac{d}{2}\right)}{2s-1}} \frac{2^{s+\frac{d}{2}-1}}{\pi^{s+\frac{d}{4}} r^{\frac{d-1}{2}}} \|f\|_{\mathcal{H}_s(\mathbb{T}^d)} N^{-s+\frac{1}{2}} + C_{f,s,d,r} N^{-s-\frac{1}{2}}$$

is valid.

Proof. Let $\mathbf{z} \in \mathbb{Z}^d$ and let $\Omega(\mathbf{z}) := \times_{j=1}^d [|z_j|, |z_j|+1]$ be the unit cube in $\mathbb{R}^d$ with "smallest" vertex at $\mathbf{z}$. Then we have for any $\mathbf{x} \in \Omega(\mathbf{z})$ the estimate $|\mathbf{z}| \geq |\mathbf{x}| - \sqrt{d}$ and, hence,

$$(1 + (2\pi)^2 |\mathbf{z}|^2)^{-s} \leq \int_{\Omega(\mathbf{z})} (1 + (2\pi)^2 (|\mathbf{x}| - \sqrt{d})^2)^{-s} \, \mathrm{d}\mathbf{x}.$$

Since f is continuous, Lemma 2.1, Inequality (7), and the Cauchy–Schwarz inequality lead to

$$\begin{aligned}
|\mathcal{M}f(\mathbf{y},r) - \mathcal{M}\mathcal{I}_N f(\mathbf{y},r)|^2 &\leq \|f - \mathcal{I}_N f\|_{L^\infty(\mathbb{T}^d)}^2 \\
&\leq 4 \left(\sum_{\mathbf{z} \in \mathbb{Z}^d \setminus J_N} \left| \hat{f}_{\mathbf{z}} \right| (1 + (2\pi)^2 |\mathbf{z}|^2)^{\frac{s}{2}} (1 + (2\pi)^2 |\mathbf{z}|^2)^{-\frac{s}{2}} \right)^2 \\
&\leq 4 \|f\|_{\mathcal{H}_s(\mathbb{T}^d)}^2 \sum_{\substack{\mathbf{z} \in \mathbb{Z}^d \\ |\mathbf{z}| \geq \frac{N}{2}}} \left(1 + (2\pi)^2 |\mathbf{z}|^2\right)^{-s} \\
&\leq 4 \|f\|_{\mathcal{H}_s(\mathbb{T}^d)}^2 \int_{|\mathbf{z}| \geq \frac{N}{2}} (1 + (2\pi)^2 (|\mathbf{z}| - \sqrt{d})^2)^{-s} \, \mathrm{d}\mathbf{z} \\
&= 4\omega_{d-1} \|f\|_{\mathcal{H}_s(\mathbb{T}^d)}^2 \int_{\frac{N}{2} - \sqrt{d}}^{\infty} \frac{(r + \sqrt{d})^{d-1}}{(1 + (2\pi)^2 r^2)^s} \, \mathrm{d}r.
\end{aligned}$$

The last integral can be simplified, since the assumption $N \geq 4\sqrt{d}$ implies $N/2 - \sqrt{d} \geq N/4$. Using moreover $r + \sqrt{d} \leq 2r$, due to $r \geq \frac{N}{2} - \sqrt{d} \geq \frac{N}{4} \geq \sqrt{d}$, and the inequality $(2\pi)^2 r^2 + 1 \geq (2\pi)^2 r^2$, we obtain

$$|\mathcal{M}f(\mathbf{y},r) - \mathcal{M}\mathcal{I}_N f(\mathbf{y},r)|^2 \leq 4\omega_{d-1} \|f\|_{\mathcal{H}_s(\mathbb{T}^d)}^2 (2\pi)^{-2s} 2^{d-1} \int_{\frac{N}{4}}^{\infty} r^{-2s+d-1} \mathrm{d}r.$$

Because of $2s - d + 1 > 1$ direct calculation in conjunction with the definition of ω_{d-1} in (1) shows the first assertion. With Equation (5) the Bessel function can be bounded by

$$\left| \mathcal{J}_{\frac{d-2}{2}}(2\pi|\mathbf{z}|r) \right| \leq \sqrt{\frac{1}{|\mathbf{z}|\pi^2 r} + C_1(d,r)|\mathbf{z}|^{-\frac{3}{2}}}, \quad C_1(d,r) > 0.$$

Thus, with $v_{\mathbf{z}}(\mathbf{x}) = \mathrm{e}^{2\pi \mathrm{i}\mathbf{z}\cdot\mathbf{x}}$ we obtain the estimate

$$\begin{aligned}
|\mathcal{M}f(\mathbf{y},r) - \mathcal{M}\mathcal{S}_N f(\mathbf{y},r)| &\le \left| \sum_{\mathbf{z}\in\mathbb{Z}^d\setminus J_N} \hat{f}_{\mathbf{z}} \left(\mathcal{M}v_{\mathbf{z}}\right)(\mathbf{y},r) \right| \\
&= \left| \sum_{\mathbf{z}\in\mathbb{Z}^d\setminus J_N} \hat{f}_{\mathbf{z}} \frac{\Gamma\left(\frac{d}{2}\right) \mathcal{J}_{\frac{d-2}{2}}(2\pi|\mathbf{z}|r)}{(\pi|\mathbf{z}|r)^{\frac{d-2}{2}}} \right| \\
&\le \frac{\Gamma\left(\frac{d}{2}\right)}{\pi^{\frac{d}{2}} r^{\frac{d-1}{2}}} \sum_{\mathbf{z}\in\mathbb{Z}^d\setminus J_N} \left|\hat{f}_{\mathbf{z}}\right| \left(|\mathbf{z}|^{\frac{1-d}{2}} + C_2(d,r)|\mathbf{z}|^{-\frac{1+d}{2}} \right),
\end{aligned}$$

and with the method of the first part of the proof we get the second assertion. For example, the first sum yields

$$\begin{aligned}
\sum_{\mathbf{z}\in J_N} \left|\hat{f}_{\mathbf{z}}\right| |\mathbf{z}|^{\frac{1-d}{2}} &\le (2\pi)^{-s} \sum_{\mathbf{z}\in\mathbb{Z}^d\setminus J_N} \left|\hat{f}_{\mathbf{z}}\right| \left(1+(2\pi)^2|\mathbf{z}|^2\right)^{\frac{s}{2}} |\mathbf{z}|^{\frac{1-d}{2}-s} \\
&\le (2\pi)^{-s} \|f\|_{\mathcal{H}_s(\mathbb{T}^d)} \left(\sum_{\mathbf{z}\in\mathbb{Z}^d\setminus J_N} |\mathbf{z}|^{1-d-2s} \right)^{\frac{1}{2}} \\
&\le \frac{\omega_{d-1}\cdot 2^{d-1}}{(2\pi)^s} \|f\|_{\mathcal{H}_s(\mathbb{T}^d)} \int_{\frac{N}{4}}^{\infty} r^{-2s} \mathrm{d}r.
\end{aligned}$$

□

An FFT-based algorithm. Next, we are concerned with fast algorithms for the approximate evaluation of spherical mean values. Combining Theorem 2.2 and Theorem 3.1 we have the following result.

Theorem 3.2. *Let $f_{\mathbf{n}} = f(\mathbf{x}_{\mathbf{n}})$, $\mathbf{n} \in I_N$, be samples of the function $f\colon \mathbb{T}^d \to \mathbb{C}$ at the regular grid $X \subset \mathbb{T}^d$ of size N^d. Then the spherical mean values*

$$g_{m_1,m_2} = \mathcal{M}\mathcal{I}_N f(\mathbf{y}_{m_1}, r_{m_2}) \approx \mathcal{M}f(\mathbf{y}_{m_1}, r_{m_2})$$

at center points $\mathbf{y}_{m_1} \in \mathbb{T}^d$, $m_1 = 1,\dots,M_1$, and radii $r_{m_2} \in (0,1]$, $m_2 = 1,\dots,M_2$, can be computed by Algorithm 1 with the numerical complexity $\mathcal{O}(M_2(N^d \log N + M_1))$.

Proof. Our algorithm starts with the computation of the Fourier coefficients

$$\hat{p}_{\mathbf{z}} = \frac{1}{N^d} \cdot \sum_{\mathbf{x}\in X} f(\mathbf{x}) \mathrm{e}^{-2\pi\mathrm{i}\mathbf{z}\cdot\mathbf{x}}, \quad \mathbf{z} \in J_N,$$

of the trigonometric interpolant $p = \mathcal{I}_N f$ by a fast Fourier transform. The numerical complexity of this first step is $\mathcal{O}(N^d \log N)$. In the second step we compute the Fourier coefficients

$$\tilde{h}_{\mathbf{z},m_2} := \hat{p}_{\mathbf{z}} \cdot \frac{\Gamma\left(\frac{d}{2}\right) \mathcal{J}_{\frac{d-2}{2}}\left(2\pi\,|\mathbf{z}|\,r_{m_2}\right)}{\left(\pi\,|\mathbf{z}|\,r_{m_2}\right)^{\frac{d-2}{2}}}, \quad \mathbf{z} \in J_N,$$

of $\mathcal{M}\mathcal{I}_N f(\cdot, r_{m_2})$ for every fixed radius r_{m_2}, $m_2 = 1,\dots,M_2$. This step has the numerical complexity $\mathcal{O}(M_2 N^d)$. In the last step we compute the spherical means

$$\mathcal{M}\mathcal{I}_N f(\mathbf{y}_{m_1}, r_{m_2}) = \sum_{\mathbf{z}\in J_N} \tilde{h}_{\mathbf{z},m_2} \mathrm{e}^{2\pi\mathrm{i}\mathbf{z}\cdot\mathbf{y}_{m_1}}, \quad m_1 = 1,\dots,M_1,$$

for every fixed radius r_{m_2} by a nonequispaced fast Fourier transform [17], which has the total numerical complexity $\mathcal{O}(M_2(N^d \log N + M_1))$. □

For the typical case that the center points are located at a $(d-1)$-dimensional submanifold of the torus $\mathbb{T}^d$ we may assume $M_1 = \mathcal{O}(N^{d-1})$ and $M_2 = \mathcal{O}(N)$. In this case our algorithm has the numerical complexity $\mathcal{O}(N^{d+1} \log N)$ which compares favorable to the numerical complexity $O(N^{2d-1})$ of a naive implementation whenever $d > 2$, see also Table 2.

Algorithm 1 Discrete spherical mean value operator

Input

$d \in \mathbb{N}$ ▷ spatial dimension

$N \in 2\mathbb{N}$, $M_1 \in \mathbb{N}$, $M_2 \in \mathbb{N}$ ▷ discretization parameter

$\mathbf{f} \in \mathbb{C}^{N^d}$ ▷ samples

$\mathbf{y}_{m_1} \in \mathbb{T}^d : m_1 = 1, \dots, M_1 - 1$ ▷ center points

$r_{m_2} \in (0, 1], m_2 = 1, \dots, M_2 - 1$ ▷ radii

Output

$\mathbf{g} \in \mathbb{C}^{M_1 M_2}$ ▷ spherical mean values

for $\mathbf{z} \in J_N$ **do**

  $\hat{p}_{\mathbf{z}} = \frac{1}{N^d} \sum_{\mathbf{x} \in X} f(\mathbf{x}) \mathrm{e}^{-2\pi \mathrm{i} \mathbf{z} \cdot \mathbf{x}}$ ▷ DFT, Eq. (6)

end for

for $m_2 = 1, ..., M_2$ **do**

  for $\mathbf{z} \in J_N \setminus \{\mathbf{0}\}$ **do**

    $\tilde{h}_{\mathbf{z},m_2} = \hat{p}_{\mathbf{z}} \cdot \frac{\Gamma\left(\frac{d}{2}\right) \mathcal{J}_{\frac{d-2}{2}}(2\pi|\mathbf{z}|r_{m_2})}{(\pi|\mathbf{z}|r_{m_2})^{\frac{d-2}{2}}}$ ▷ multiplier

  end for

  $\tilde{h}_{\mathbf{0},m_2} := \hat{f}_{\mathbf{0}}$

  for $m_1 = 1, \dots, M_1$ **do**

    $g_{m_1,m_2} := \sum_{\mathbf{z} \in J_N} \tilde{h}_{\mathbf{z},m_2} \mathrm{e}^{2\pi \mathrm{i} \mathbf{z} \cdot \mathbf{y}_{m_1}}$ ▷ NDFT

  end for

end for

A fast algorithm for the three-dimensional case. Let us now consider the practical important case $d = 3$. Then the discrete spherical mean value operator can be written in terms of a sparse four-dimensional Fourier transform. To be more precise, we define the following discrete subset

$$\tilde{J}_N := \left\{ (\mathbf{z}, \zeta) \in J_N \times \left[-\frac{\sqrt{3}N}{2}, \frac{\sqrt{3}N}{2} \right] : |\zeta| = |\mathbf{z}| \right\} \setminus \{\mathbf{0}\} \tag{8}$$

of a three-dimensional double cone in $\mathbb{R}^4$.

Theorem 3.3. *Let $d = 3$, $N \in \mathbb{N}$, and $p \in T_N$,*

$$p(\mathbf{x}) = \sum_{\mathbf{z} \in J_N} \hat{p}_{\mathbf{z}} \mathrm{e}^{2\pi \mathrm{i} \mathbf{z} \cdot \mathbf{x}},$$

be a trigonometric polynomial. Then its spherical mean values at center points $\mathbf{y} \in \mathbb{T}^d$ *and radii* $r > 0$ *have the representation*

$$\mathcal{M}p(\mathbf{y}, r) = \hat{p}_{\mathbf{0}} - \frac{\mathrm{i}}{4\pi r} \sum_{(\mathbf{z},\zeta)\in\tilde{J}_N} \frac{\hat{p}_{\mathbf{z}}}{\zeta} \cdot \mathrm{e}^{2\pi\mathrm{i}(\mathbf{z},\zeta)\cdot(\mathbf{y},r)}. \tag{9}$$

Proof. First of all we observe that for all $\mathbf{z} \in J_N\backslash\{\mathbf{0}\}$ and $r > 0$ the identity

$$\frac{\Gamma\left(\frac{3}{2}\right)\mathcal{J}_{\frac{1}{2}}(2\pi\,|\mathbf{z}|\,r)}{\sqrt{\pi\,|\mathbf{z}|\,r}} = \frac{\sin 2\pi\,|\mathbf{z}|\,r}{2\pi\,|\mathbf{z}|\,r} = \frac{-\mathrm{i}}{4\pi\,|\mathbf{z}|\,r}\left(\mathrm{e}^{2\pi\mathrm{i}|\mathbf{z}|r} - \mathrm{e}^{-2\pi\mathrm{i}|\mathbf{z}|r}\right) \tag{10}$$

holds true. Hence, we have by Theorem 2.2

$$\begin{aligned}
\mathcal{M}p(\mathbf{y}, r) &= \sum_{\mathbf{z}\in J_N} \hat{p}_{\mathbf{z}} \cdot \left(\mathcal{M}\mathrm{e}^{2\pi\mathrm{i}\mathbf{z}\cdot(\cdot)}\right)(\mathbf{y}, r) \\
&= \hat{p}_{\mathbf{0}} + \sum_{\mathbf{z}\in J_N\backslash\{\mathbf{0}\}} \hat{p}_{\mathbf{z}} \cdot \mathrm{e}^{2\pi\mathrm{i}\mathbf{z}\cdot\mathbf{y}} \cdot \frac{\Gamma\left(\frac{3}{2}\right)\mathcal{J}_{\frac{1}{2}}(2\pi\,|\mathbf{z}|\,r)}{\sqrt{\pi\,|\mathbf{z}|\,r}} \\
&= \hat{p}_{\mathbf{0}} + \frac{-\mathrm{i}}{4\pi r} \cdot \sum_{\mathbf{z}\in J_N\backslash\{\mathbf{0}\}} \frac{\hat{p}_{\mathbf{z}}}{|\mathbf{z}|} \cdot \mathrm{e}^{2\pi\mathrm{i}\mathbf{z}\cdot\mathbf{y}} \cdot (\mathrm{e}^{2\pi\mathrm{i}|\mathbf{z}|r} - \mathrm{e}^{-2\pi\mathrm{i}|\mathbf{z}|r}).
\end{aligned}$$

□

Next we assume that the center points $\mathbf{y}_{m_1}$, $m_1 = 1, \ldots, M_1$, are restricted to a smooth two-dimensional submanifold of $\mathbb{T}^3$. Then for arbitrary radii r_{m_2}, $m_2 = 1, \ldots, M_2$, the set of nodes $(\mathbf{y}_{m_1}, r_{m_2}) \in \mathbb{R}^4$, $m_1 = 1, \ldots, M_1$, $m_2 = 1, \ldots, M_2$, lies on a smooth three-dimensional submanifold of $\mathbb{R}^4$. Hence, Equation (9) describes a four-dimensional Fourier transform with Fourier coefficients as well as evaluation nodes on smooth three-dimensional submanifolds. Such a sparse Fourier transform can be computed efficiently, cf. [28, 19], using the following two main ingredients. At first, we employ a low rank approximation $\mathrm{e}^{2\pi\mathrm{i}(\mathbf{z},\zeta)\cdot(\mathbf{y},r)} = \sum_{\ell=1}^{R} a_\ell(\mathbf{z},\zeta)b_\ell(\mathbf{y},r)$ of the Fourier kernel, where the rank fulfills $R \approx \log^4(N/\varepsilon)$ under certain conditions on the widths of the spatial and frequency domains. In order to meet these conditions, the second ingredient is a dyadic subdivision of both domains, resulting in a particular divide and conquer strategy, the so-called butterfly scheme.

The following Corollary 1 and Algorithm 2 summarize its application to the computation of spherical means.

Corollary 1. *Let* $f\colon \mathbb{T}^3 \to \mathbb{C}$ *be sampled on the regular grid* X *of size* N^3 *and let the center points* $\mathbf{y}_{m_1}$, $m_1 = 1, \ldots, M_1$, *be located at a two-dimensional submanifold of* $\mathbb{T}^3$. *Moreover, let the radii* $r_{m_2} \in (0, 1]$, $m_2 = 1, \ldots, M_2$, *be given and assume* $M_1 = \mathcal{O}(N^2)$ *and* $M_2 = \mathcal{O}(N)$. *Then the evaluation of the approximated spherical mean values*

$$g_{m_1,m_2} = \mathcal{M}\mathcal{I}_N f(\mathbf{y}_{m_1}, r_{m_2}) \approx \mathcal{M}f(\mathbf{y}_{m_1}, r_{m_2}), \quad m_2 = 1, \ldots, M_2,\ m_2 = 1, \ldots, M_2,$$

by Algorithm 2 has the numerical complexity $\mathcal{O}(N^3 \log^6 N)$.

Proof. As in Algorithm 1 we first compute the Fourier coefficients $\hat{p}_{\mathbf{z}}$, $\mathbf{z} \in J_N$, of the trigonometric interpolant $\mathcal{I}_N f$. Next, the coefficients for the sparse Fourier transform are computed by

$$\hat{h}_{\mathbf{z},\zeta} := \frac{\hat{p}_{\mathbf{z}}}{\zeta}, \quad (\mathbf{z}, \zeta) \in \tilde{J}_N. \tag{11}$$

Finally, the sparse Fourier transform

$$g_{m_1,m_2} = \hat{p}_{\mathbf{0}} - \frac{\mathrm{i}}{4\pi r} \sum_{(\mathbf{z},\zeta)\in\tilde{J}_N} \hat{h}_{\mathbf{z},\zeta} \mathrm{e}^{2\pi\mathrm{i}(\mathbf{z},\zeta)\cdot(\mathbf{y}_{m_1},r_{m_2})},\ m_1 = 1,\dots,M_1,\ m_2 = 1,\dots,M_2,$$

is computed by the algorithm described in [19] which results in a total complexity of $\mathcal{O}(N^3 \log^6 N)$. □

Algorithm 2 Discrete spherical mean value operator, using sparse FFT, $d = 3$

1: **Input** and **Output** as in Algorithm 1

2: **for** $\mathbf{z} \in J_N$ **do**
3: $\quad \hat{p}_{\mathbf{z}} = \frac{1}{N^3} \sum_{\mathbf{x}\in X} f(\mathbf{x}) \mathrm{e}^{-2\pi\mathrm{i}\mathbf{z}\cdot\mathbf{x}}$ ▷ DFT, Eq. (6)
4: **end for**
5: **for** $(\mathbf{z},\zeta) \in \tilde{J}_N$ **do**
6: $\quad \hat{h}_{\mathbf{z},\zeta} := \frac{\hat{p}_{\mathbf{z}}}{\zeta}$ ▷ coefficients for sparse FFT, Eq. (11)
7: **end for**
8: **for** $m_1 = 1,\dots,M_1$ **do**
9: $\quad$ **for** $m_2 = 1,\dots,M_2$ **do**
10: $\quad\quad g_{m_1,m_2} = \hat{p}_{\mathbf{0}} - \frac{\mathrm{i}}{4\pi r} \sum_{(\mathbf{z},\zeta)\in\tilde{J}_N} \hat{h}_{\mathbf{z},\zeta} \cdot \mathrm{e}^{2\pi\mathrm{i}(\mathbf{z},\zeta)\cdot(\mathbf{y}_{m_1},r_{m_2})}$ ▷ sparse FFT, Eq. (9)
11: $\quad$ **end for**
12: **end for**

A comparison between the complexities of the Algorithms 1, 2 and a naive algorithm based on a piecewise polynomial approximation can be found in Table 2.

4. **Numerical Experiments.** In this section, we analyze numerical results of the presented discretizations of the spherical mean value operator. In particular, we consider the approximation errors and the running times. The algorithms are implemented in Matlab and the numerical results were obtained on an Intel Xeon E7450 with 2.4 GHz and 94 GByte RAM running Matlab R2010b.

Let us start by defining some test functions. Let a size parameter $t \in (0, 0.5]$, a smoothness parameter $s \in \mathbb{N}_0$, and the radial test function $f_{d,s,t} : \mathbb{R}^d \to \mathbb{R}$,

$$f_{d,s,t}(\mathbf{x}) := \begin{cases} \varphi_{s,t}\left(|\mathbf{x}|^2\right) & |\mathbf{x}| \le t, \\ 0 & \text{otherwise}, \end{cases} \qquad \varphi_{s,t}(\tau) := \left(1 - \frac{\tau}{t^2}\right)^s, \tag{12}$$

be given. We compute spherical means of these test functions analytically by using the following statement for radial functions.

Lemma 4.1. *Let a spatial dimension $d \in \mathbb{N}$, $d \ge 2$, a center point $\mathbf{y} \in \mathbb{R}^d$, a radius $r \ge 0$, and a radial function $f : \mathbb{R}^d \to \mathbb{R}$, $f(\mathbf{x}) = \varphi\left(|\mathbf{x}|^2\right)$ for some function $\varphi\colon [0,\infty) \to \mathbb{R}$, be given. Then the spherical mean values of the function f can be computed by*

$$\mathcal{M}f(\mathbf{y}, r) = \frac{\omega_{d-2}}{\omega_{d-1}} \int_{-1}^{1} \varphi\left(|\mathbf{y}|^2 + r^2 + 2r|\mathbf{y}|\tau\right) \left(1 - \tau^2\right)^{\frac{d-3}{2}} \mathrm{d}\tau.$$

Proof. First assume without loss of generality $\mathbf{y} = |\mathbf{y}|\,\mathbf{e}_d$, where $\mathbf{e}_d = (0,\dots,0,1)^\top \in \mathbb{R}^d$. Then

$$\begin{aligned}\mathcal{M}f(\mathbf{y},r) &= \frac{1}{\omega_{d-1}}\int_{\mathbb{S}^{d-1}} \varphi\left(|\mathbf{y}+r\boldsymbol{\xi}|^2\right)\mathrm{d}\sigma(\boldsymbol{\xi}) \\ &= \frac{1}{\omega_{d-1}}\int_{\mathbb{S}^{d-1}} \varphi\left(|\mathbf{y}|^2+r^2+2r\,|\mathbf{y}|\,\boldsymbol{\xi}\cdot\mathbf{e}_d\right)\mathrm{d}\sigma(\boldsymbol{\xi}) \\ &= \frac{1}{\omega_{d-1}}\int_{-1}^{1}\int_{\mathbb{S}^{d-2}} \varphi\left(|\mathbf{y}|^2+r^2+2r|\mathbf{y}|\tau\right)\mathrm{d}\sigma(\tilde{\boldsymbol{\xi}})(1-\tau^2)^{\frac{d-3}{2}}\,\mathrm{d}\tau.\end{aligned}$$

□

Next we use the above lemma to compute the spherical mean values of some of the test functions (12) explicitly.

Example 4.2. Let us start with spatial dimension $d = 2$. Then we have

$$\mathcal{M}f_{2,s,t}(\mathbf{y},r) = \frac{1}{\pi}\int_0^{\vartheta_0} \varphi_{s,t}\left(|\mathbf{y}|^2+r^2-2r|\mathbf{y}|\cos\vartheta\right)\mathrm{d}\vartheta,$$

where

$$\vartheta_0 := \vartheta_0\left(|\mathbf{y}|,r,t\right) := \begin{cases}\pi & \text{for} \quad t^2 \geq (|\mathbf{y}|+r)^2, \\ 0 & \text{for} \quad t^2 < (|\mathbf{y}|-r)^2, \\ \arccos\frac{|\mathbf{y}|^2+r^2-t^2}{2r|\mathbf{y}|} & \text{else.}\end{cases}$$

Fixing the smoothness parameter $s \in \mathbb{N}_0$ gives an explicit solution of the integral. With adequate coefficients $b_{s,k} := b_{s,k}(\mathbf{y},r,t) \in \mathbb{R}$, $k = 0,\ldots,s$, we have

$$\varphi_{s,t}\left(|\mathbf{y}|^2+r^2-2r|\mathbf{y}|\cos\vartheta\right) = \sum_{k=0}^{s} b_{s,k}(\cos\vartheta)^k$$

and it follows

$$\mathcal{M}f_{2,s,t}(\mathbf{y},r) = \frac{1}{\pi}\sum_{k=0}^{s} b_{s,k}\int_0^{\vartheta_0}(\cos\vartheta)^k\mathrm{d}\vartheta.$$

For example $s = 0$ yields the coefficient $b_{0,0} = 1$ and $s = 1$ yields the coefficients $b_{1,0} = \frac{t^2-|\mathbf{y}|^2-r^2}{t^2}$ and $b_{1,1} = \frac{2r|\mathbf{y}|}{t^2}$. Hence, we obtain

$$\mathcal{M}f_{2,0,t}(\mathbf{y},r) = \frac{\vartheta_0}{\pi} \quad \text{and}$$

$$\mathcal{M}f_{2,1,t}(\mathbf{y},r) = \frac{1}{\pi}\left(b_{1,0}\cdot\vartheta_0 + b_{1,1}\cdot\sin\vartheta_0\right) = \frac{\vartheta_0\cdot\left(t^2-|\mathbf{y}|^2-r^2\right)+2r|\mathbf{y}|\sin\vartheta_0}{\pi t^2}.$$

Example 4.3. Since the weight disappears for dimension $d = 3$ we define a primitive $\Phi_{s,t} : \mathbb{R} \to \mathbb{R}$ of $\varphi_{s,t}$ and an auxiliary quantity $\tau_0 \in \mathbb{R}_+$,

$$\Phi_{s,t}(\tau) := -\frac{\left(t^2-\tau\right)^{s+1}}{t^{2s}\,(1+s)}, \quad \tau_0 := \begin{cases}\left(|\mathbf{y}|+r\right)^2 & \text{for} \quad t^2 \geq \left(|\mathbf{y}|+r\right)^2, \\ \left(|\mathbf{y}|-r\right)^2 & \text{for} \quad t^2 < \left(|\mathbf{y}|-r\right)^2, \\ t^2 & \text{otherwise,}\end{cases}$$

and obtain for $\mathbf{y} \neq \mathbf{0}$ and $r \neq 0$ the closed-form expression

$$\mathcal{M}f_{3,s,t}(\mathbf{y},r) = \frac{1}{4r|\mathbf{y}|}\cdot\left(\Phi_{s,t}(\tau_0) - \Phi_{s,t}\left(\left(|\mathbf{y}|-r\right)^2\right)\right).$$

For example with parameters $s = 0$ and $s = 1$ we get the formulas

$$\mathcal{M}f_{3,0,t} = \frac{\tau_0 - (|\mathbf{y}| - r)^2}{4r|\mathbf{y}|}, \quad \mathcal{M}f_{3,1,t} = \frac{\left(t^2 - (|\mathbf{y}| - r)^2\right)^2 - \left(t^2 - \tau_0\right)^2}{8r|\mathbf{y}|t^2}.$$

Moreover, Sonine's integral [27, Chapter 12.11] yields the Fourier transform of these test functions

$$\hat{f}_{d,s,t}(\mathbf{z}) = \frac{\Gamma(s+1)t^{\frac{d}{2}-s}}{\pi^s} \cdot \frac{\mathcal{J}_{s+\frac{d}{2}}(2\pi\,|\mathbf{z}|\,t)}{|\mathbf{z}|^{s+\frac{d}{2}}}, \tag{13}$$

which, in conjunction with [27, Sec. 7.21], allows for the estimate

$$\left|\hat{f}_{d,s,t}(\mathbf{z})\right| \leq C_{d,s,t} \cdot (1 + |\mathbf{z}|^2)^{-\frac{1}{2}\left(s+\frac{d+1}{2}\right)} \tag{14}$$

and thus $f_{d,s,t} \in \mathcal{H}_{s+\frac{1}{2}-\varepsilon}(\mathbb{T}^d)$ for every $\varepsilon > 0$. Theorem 3.1 implies

$$\begin{aligned} &|\mathcal{M}f_{d,s,t}(\mathbf{y},r) - \mathcal{M}\mathcal{I}_N f_{d,s,t}(\mathbf{y},r)| \leq C_{d,s,t,f,\varepsilon} \cdot N^{\frac{d}{2}-s-\frac{1}{2}+\varepsilon} \quad \text{and} \\ &|\mathcal{M}f_{d,s,t}(\mathbf{y},r) - \mathcal{M}\mathcal{S}_N f_{d,s,t}(\mathbf{y},r)| \leq C_{d,s,t,f,\varepsilon} \cdot N^{-s+\varepsilon}. \end{aligned}$$

Additionally to the Algorithms 1 and 2 we consider also a variant that makes use of the exact Fourier coefficients (13) of our test functions and implements $\mathcal{M}S_N f$. This algorithm is labeled as Algorithm 1a in the following tables and figures.

Furthermore, we consider two algorithms that are based on piecewise polynomial approximation. In the most simplest case the function f is approximated by a piecewise constant function and a simple rectangular quadrature rule is applied, see Algorithm 3. A variant using bilinear interpolation and a trapezoidal quadrature rule is subsequently labeled as Algorithm 3a.

Algorithm 3 Discrete spherical mean value operator, naive scheme, $d = 2$

Input and **Output** as in Algorithm 1

for $m_2 = 1, ..., M_2$ **do**
  $n := \lceil 2\pi r_{m_2} N \rceil$ ▷ number of sampling points
  for $m_1 = 1, ..., M_1$ **do**
    $s := 0$
    for $l = 0, ..., n-1$ **do**
      $\varphi_l := \frac{2\pi l}{n}$
      $\mathbf{x}_l := \mathbf{y}_{m_1} + r_{m_2} \begin{pmatrix} \cos\varphi_l \\ \sin\varphi_l \end{pmatrix}$ ▷ sampling point
      $\widetilde{\mathbf{x}}_l := \left(\frac{2\left\lfloor (\mathbf{x}_l)_1 \cdot N + \frac{N}{2} - \frac{1}{2} \right\rfloor + 1 - N}{2N}, \frac{2\left\lfloor (\mathbf{x}_l)_2 \cdot N + \frac{N}{2} - \frac{1}{2} \right\rfloor + 1 - N}{2N} \right)^\top$ ▷ nearest grid p.
      $s := s + f\left(\widetilde{\mathbf{x}}_l\right)$
    end for
    $g_{m1,m2} := \frac{1}{n} \cdot s$
  end for
end for

We compare the approximation error of the Algorithms 1, 1a, 3, and 3a with respect to the discretization parameter N. Therefore, we fix the test function $f_{s,t,d}$ with smoothness parameter $s = 3$, size parameter $t = \frac{1}{5}$, dimension $d = 2, 3$, and center points $\mathbf{y}_{m_1} \in \mathbb{T}^d$,

$m_1 = 1 \dots, M_1$, and radii $r_{m_2} \in (0, 1]$, $m_2 = 1 \dots, M_2$. For this setting we plot the maximum error

$$\varepsilon_{\text{abs}} = \max_{m_1=1,\dots,M_1} \max_{m_2=1,\dots,M_2} \left| \left(\mathcal{M} f_{d,s,t}\right)(\mathbf{y}_{m_1}, r_{m2}) - g(\mathbf{y}_{m_1}, r_{m_2}) \right|,$$

where $g(\mathbf{y}_{m_1}, r_{m_2})$ is the result of one of the algorithms. The results are plotted in Figure 1 which clearly confirms the superior error rate of the Fourier based discretization compared to the discretization by piecewise polynomial functions. Table 1 summarizes the numerical and theoretical convergence rates with respect to the smoothness parameter s. This indicates that the convergence rate of the Fourier based algorithms for the considered test functions is even better than the theoretical bound proven in Theorem 3.1. We suspect that this is related to the fact, that the Fourier coefficients of $f_{s,t,d}$ oscillate.

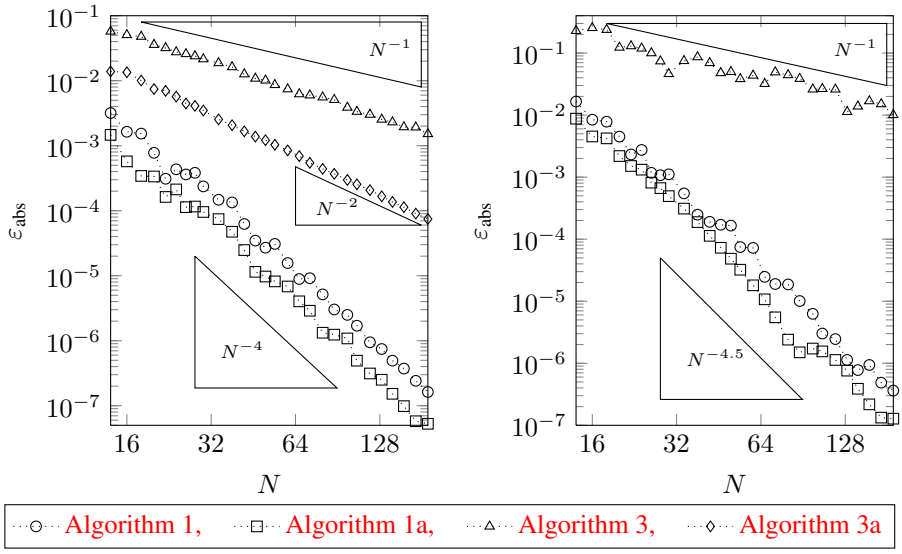

FIGURE 1. Accuracy with respect to the discretization parameter N for spatial dimension $d = 2$ (left) and $d = 3$ (right), and test functions with smoothness parameter $s = 3$.

Next we are going to compare the running times of our algorithms. Therefore, we consider the practical important case that the center points $\mathbf{y}_1, \dots, \mathbf{y}_{M_1} \in \mathbb{T}^d$, $M_1 = \mathcal{O}(N^{d-1})$, are located on the surface of a cylinder and that the radii $r_1, \dots, r_{M_2} \in (0, 1]$, $M_2 = \mathcal{O}(N)$, are equispaced. The numerical complexities of our algorithms for this setting are summarized in Table 2. The numerical results are shown in Figure 2. We observe that in the two-dimensional case we have nearly the same behavior for all algorithms. In the three-dimensional case, however, the algorithm based on the NFFT is much faster than the naive algorithm. This speedup is essential for practical applications where N is large. Since the NFFT based algorithm is implemented in C its absolute running time is much better compared to the sparse Fourier transform based algorithm which is implemented in Matlab. Nevertheless, the sparse Fourier transform based algorithm shows the slowest increase of the running time as N grows. More sophisticated implementations of the sparse Fourier transform are subject of current research.

	$d=2$				$d=3$		
s	Alg. 3	Alg. 3a	Alg. 1	Alg. 1a	Alg. 3	Alg. 1	Alg. 1a
0	0.76	0.60	0.83	0.88	1.10	1.12	1.37
1	1.25	1.55	1.79	1.97	1.10	2.03	2.45
2	1.34	2.04	2.86	3.03	1.06	3.23	3.29
3	1.42	2.06	3.78	3.89	1.10	4.21	4.49
4	1.37	2.00	4.84	5.02	1.14	5.40	5.41
5	1.32	1.96	5.75	5.91	1.18	6.42	6.57
6	1.30	1.95	6.68	6.92	1.24	7.40	7.49
conjecture	1	2	$s+1$	$s+1$	1	$s+1.5$	$s+1.5$
theory	–	–	$s-0.5$	s	–	$s-1$	s

TABLE 1. Estimated orders $-\log \varepsilon_{\text{abs}}/\log N$ of convergence with respect to the smoothness parameter s. These are derived by a least square fit of the computed errors in Figure 1.

Spatial dimension	2	3
Input and output data	$\mathcal{O}\left(N^2\right)$	$\mathcal{O}\left(N^3\right)$
Algorithm	arithmetic operations	
Naive implementation, Alg. 3	$\mathcal{O}\left(N^3\right)$	$\mathcal{O}\left(N^5\right)$
Fourier method, using NFFT, Alg. 1	$\mathcal{O}\left(N^3 \log N\right)$	$\mathcal{O}\left(N^4 \log N\right)$
Fourier method, using sparse FFT, Alg. 2	–	$\mathcal{O}\left(N^3 \log^6 N\right)$

TABLE 2. Complexities of the algorithms for spatial dimensions $d=2$ and $d=3$.

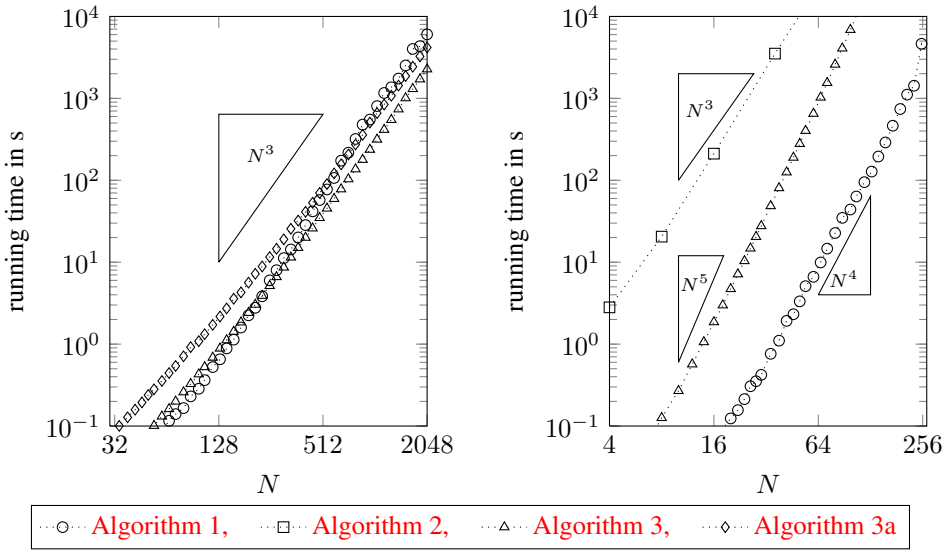

FIGURE 2. Running times with respect to the discretization parameter N for spatial dimension $d=2$ (left) and $d=3$ (right).

5. **Summary.** We discretized the spherical mean value operator by trigonometric polynomials, which gives rise to spectral error estimates in case of globally smooth functions. Moreover, the resulting algorithm has optimal arithmetical complexity in the important three-dimensional case and thus allows for the computation of spherical mean values for large problem sizes.

Acknowledgments. The authors thank the reviewers for their valuable suggestions and gratefully acknowledge support by the German Research Foundation within the project KU 2557/1-2 and by the Helmholtz Association within the young investigator group VH-NG-526.

REFERENCES

[1] M. Agranovsky and P. Kuchment. Uniqueness of reconstruction and an inversion procedure for thermoacoustic and photoacoustic tomography with variable sound speed. *Inverse Problems*, 23(5):2089–2102, 2007.

[2] M. Agranovsky, P. Kuchment, and L. Kunyansky. On reconstruction formulas and algorithms for the thermoacoustic tomography. In L. V. Wang, editor, *Photoacoustic imaging and spectroscopy*, chapter 8, pages 89–101. CRC Press, Boca Raton, FL, 2009.

[3] M. Agranovsky, P. Kuchment, and E. T. Quinto. Range descriptions for the spherical mean Radon transform. *J. Funct. Anal.*, 248(2):344–386, 2007.

[4] A. Buehler, A. Rosenthal, T. Jetzfellner, A. Dima, D. Razansky, and V. Ntziachristos. Model-based optoacoustic inversions with incomplete projection data. *Med. Phys.*, 38(1694), 2011.

[5] P. Burgholzer, G. J. Matt, M. Haltmeier, and G. Paltauf. Exact and approximate imaging methods for photoacoustic tomography using an arbitrary detection surface. *Phys. Rev. E*, 75(4):046706, 2007.

[6] Y. Dong, T. Görner, and S. Kunis. An iterative reconstruction scheme for photoacoustic imaging. *Preprint*, 2011.

[7] F. Filbir, R. Hielscher, and W. R. Madych. Reconstruction from circular and spherical mean data. *Appl. Comput. Harmon. Anal.*, 29(1):111–120, 2010.

[8] D. Finch, M. Haltmeier, and Rakesh. Inversion of spherical means and the wave equation in even dimensions. *SIAM J. Appl. Math.*, 68(2):392–412, 2007.

[9] M. Haltmeier. A mollification approach for inverting the spherical mean Radon transform. *SIAM J. Appl. Math.*, 71(5):1637–1652, 2011.

[10] M. Haltmeier. Inversion of circular means and the wave equation on convex planar domains. *ArXiv e-prints*, 2012.

[11] M. Haltmeier. Universal inversion formulas for recovering a function from spherical means. *ArXiv e-prints*, 2012.

[12] M. Haltmeier, O. Scherzer, P. Burgholzer, and G. Paltauf. Thermoacoustic computed tomography with large planar receivers. *Inverse Problems*, 20(5):1663–1673, 2004.

[13] M. Haltmeier, O. Scherzer, and G. Zangerl. A reconstruction algorithm for photoacoustic imaging based on the nonuniform FFT. *IEEE Trans. Med. Imag.*, 28(11):1727–1735, 2009.

[14] M. Haltmeier, T. Schuster, and O. Scherzer. Filtered backprojection for thermoacoustic computed tomography in spherical geometry. *Math. Methods Appl. Sci.*, 28(16):1919–1937, 2005.

[15] M. Haltmeier and G. Zangerl. Spatial resolution in photoacoustic tomography: effects of detector size and detector bandwidth. *Inverse Problems*, 26(12):125002, 14, 2010.

[16] F. John. *Plane waves and spherical means applied to partial differential equations*. Dover Publications Inc., Mineola, NY, 2004. Reprint of the 1955 original.

[17] J. Keiner, S. Kunis, and D. Potts. Using NFFT 3—a software library for various nonequispaced fast Fourier transforms. *ACM Trans. Math. Software*, 36(4):Art. 19, 30, 2009.

[18] P. Kuchment and L. Kunyansky. Mathematics of thermoacoustic tomography. *European J. Appl. Math.*, 19(2):191–224, 2008.

[19] S. Kunis and I. Melzer. A stable and accurate butterfly sparse Fourier transform. *SIAM J. Numer. Anal.*, 50(3):1777–1800, 2012.

[20] L. Kunyansky. Reconstruction of a function from its spherical (circular) means with the centers lying on the surface of certain polygons and polyhedra. *Inverse Problems*, 27(2):025012, 22, 2011.

[21] L. A. Kunyansky. Explicit inversion formulae for the spherical mean Radon transform. *Inverse Problems*, 23(1):373–383, 2007.

[22] L. A. Kunyansky. A series solution and a fast algorithm for the inversion of the spherical mean Radon transform. *Inverse Problems*, 23(6):S11–S20, 2007.

[23] F. Natterer. Photo-acoustic inversion in convex domains. *Inverse Probl. Imaging*, 6(2):1–6, 2012.
[24] G. Paltauf, R. Nuster, M. Haltmeier, and P. Burgholzer. Photoacoustic tomography with integrating area and line detectors. In L. V. Wang, editor, *Photoacoustic Imaging and Spectroscopy*, Optical Science and Engineering, chapter 20, pages 251–263. CRC Press, Boca Raton, FL, 2009.
[25] E. T. Quinto. Helgason's support theorem and spherical Radon transforms. In *Radon transforms, geometry, and wavelets*, volume 464 of *Contemp. Math.*, pages 249–264. Amer. Math. Soc., Providence, RI, 2008.
[26] L. V. Wang and H. Wu. *Biomedical Optics - Principles and Imaging*. John Wiley & Sons Inc., Hoboken, NJ, 2007.
[27] G. N. Watson. *A Treatise on the Theory of Bessel Functions*. Cambridge University Press, Cambridge, GB, 1966.
[28] L. Ying. Sparse Fourier transform via butterfly algorithm. *SIAM J. Sci. Comput.*, 31(3):1678–1694, 2009.
[29] G. Zangerl and O. Scherzer. Exact reconstruction in photoacoustic tomography with circular integrating detectors II: spherical geometry. *Math. Methods Appl. Sci.*, 33(15):1771–1782, 2010.
[30] G. Zangerl, O. Scherzer, and M. Haltmeier. Exact series reconstruction in photoacoustic tomography with circular integrating detectors. *Commun. Math. Sci.*, 7(3):665–678, 2009.
[31] A. Zygmund. *Trigonometric series. Vol. I, II*. Cambridge Mathematical Library. Cambridge University Press, Cambridge, third edition, 2002. With a foreword by Robert A. Fefferman.

E-mail address: torsten.goerner@uos.de
E-mail address: ralf.hielscher@mathematik.tu-chemnitz.de
E-mail address: stefan.kunis@math.uos.de